JAAS

ROYAL SOCIETY OF CHEMISTRY

PAPER

Cite this: *J. Anal. At. Spectrom.*, 2023, **38**, 437

In situ Hf isotope analysis of cassiterite by LA-MC-ICP-MS: protocol and applications†

Ming Yang, [abc] Yue-Heng Yang, *[bc] Rolf L. Romer,[d] Shi-Tou Wu, [bc] Tao Wu[ae] and Hao Wang [bc]

Received 20th October 2022
Accepted 12th December 2022

DOI: 10.1039/d2ja00340f

rsc.li/jaas

We report the laser ablation multi-collector inductively coupled plasma mass spectrometry (LA-MC-ICP-MS) $^{176}Hf/^{177}Hf$ ratios for cassiterite of a known age and demonstrate that the $^{176}Hf/^{177}Hf$ ratios can be measured accurately and reproducibly with adequate precision for cassiterite with Hf contents around 100 μg g^{-1}. Although cassiterite only has minor rare earth elements (REEs), corrections for Yb and Lu interferences are required as they may affect the determination of the $^{176}Hf/^{177}Hf$ ratios. Among the investigated samples, Rond-A has a homogeneous Hf isotopic composition. We recommend cassiterite sample Rond-A as a primary reference material for *in situ* Hf isotope analysis. The Kard sample has a homogeneous Hf isotopic composition and is suitable as a primary reference material once its Hf isotopic composition has been confirmed by solution-based MC-ICP-MS. Samples BB#7, 19MP, and 19GX showed minor variations in their Hf isotopic compositions and, therefore, can only be used as secondary reference materials.

1. Introduction

The Lu–Hf isotopic system is a powerful geochemical tool to trace the contributions of isotopically contrasting crust and mantle materials in magmatic rocks, such as the recycling of crustal material into the mantle or the involvement of mantle-derived melts in highly evolved magmas.[1–4] As the thermal ionization mass spectrometry (TIMS) measurement procedure is rather challenging,[1] the Lu–Hf system was initially not widely used. However, the application of the Lu–Hf method later became more widespread for bulk rock samples with the availability of MC-ICP-MS instruments and then experienced an additional boost with the development of *in situ* analysis using LA-MC-ICP-MS for Hf-rich minerals, such as zircon and baddeleyite.[5] The high spatial resolution of *in situ* analysis allows the determination of the isotopic composition of individual growth zones within minerals.[6–8] With the development of analytical equipment, *in situ* Hf isotope analysis has been expanded to include minerals with low to moderate Hf contents, such as rutile,[9,10] columbite group minerals,[11,12] and cassiterite.[11] Using *in situ* Hf isotope analysis on ore minerals such as cassiterite provides an unprecedented opportunity to fingerprint the metal source of tin mineralization by analyzing the ore mineral directly.

Cassiterite, the most important ore mineral in tin deposits, has been used to determine the age of magmatic and hydrothermal tin mineralization and tin redistribution, as well as the crystallization age of cassiterite-bearing pegmatites.[13–18] Cassiterite has the tetragonal lattice structure of rutile group minerals ($M^{4+}O_2$).[16,19,20] This lattice structure can accommodate isomorphically large quantities of trace elements, such as Sc, Ti, V, Mn, Fe, Nb, Ta, Zr, Hf, Sb, and W.[18–21] The contents of rare earth elements (REEs) of cassiterite tend to be minor and the Yb/Hf and Lu/Hf ratios are generally very low,[19,20] making cassiterite a promising mineral for *in situ* Hf isotope analysis. Kendall-Langley *et al.*[11] presented the first *in situ* Hf isotope data of cassiterite using the LA-MC-ICP-MS technique. However, the laser ablation analysis was not checked by solution-based methods. Most of the analyses obtained gave $^{176}Hf/^{177}Hf$ ratios for cassiterite that agreed well with published whole rock or zircon values.

In situ Hf isotope analysis of cassiterite benefits from the same advantage as *in situ* zircon Hf isotope analysis. These minerals have low Lu/Hf ratios, which implies that the isotopic composition of Hf incorporated at the time of crystallization of the mineral does not change appreciably and can provide reliable source information. *In situ* cassiterite Hf isotope analysis, however, faces several analytical problems that do not occur for

[a]*Hainan Institute of Zhejiang University, Sanya, Hainan Province, 572025, P. R. China*
[b]*State Key Laboratory of Lithospheric Evolution, Institute of Geology and Geophysics, Chinese Academy of Sciences, Beijing, 100029, P. R. China. E-mail: yangyueheng@mail.iggcas.ac.cn*
[c]*Institutions of Earth Sciences, Chinese Academy of Sciences, Beijing, 100029, P. R. China*
[d]*GFZ German Research Centre for Geosciences, Telegrafenberg, Potsdam, 14473, Germany*
[e]*Ocean College, Zhejiang University, Zhoushan, Zhejiang Province, 316021, P. R. China*

† Electronic supplementary information (ESI) available. See DOI: https://doi.org/10.1039/d2ja00340f

zircon and that need to be resolved, including: (i) *in situ* analysis requires matrix-matched reference materials. There is, however, no matrix-matched reference material available for *in situ* cassiterite Hf isotope analysis; (ii) the content of Hf is relatively low (<400 μg g^{-1});[11] (iii) although, the Yb/Hf and Lu/Hf ratios of cassiterite typically are very low,[19,20] it is not clear whether the isobaric interferences of Yb and Lu have an effect on *in situ* Hf analysis.

This work has the following objectives: (i) establish a procedure for the *in situ* Hf isotope measurement of cassiterite by LA-MC-ICP-MS; (ii) investigate the effect of the isobaric interferences of ^{176}Yb and ^{176}Lu on ^{176}Hf measurement; and (iii) develop cassiterite reference materials suitable for *in situ* Hf isotope measurement.

2. Analytical techniques

All the cassiterite grains to be tested were concentrated using a Frantz magnetic separator and heavy liquids and selected by hand picking under a binocular microscope. Some cassiterite grains were embedded in a 1-inch epoxy mount, sectioned to expose their interior, polished, and mapped by optical microscopy. The Hf isotopic homogeneity of the cassiterite samples were tested by LA-MC-ICP-MS analysis. For the samples to be used for the solution-based MC-ICP-MS Hf isotope measurement, handpicked cassiterite grains were pulverized (about 200 mesh) prior to analysis.

2.1 *In situ* trace element analysis

All the trace element analyses were performed at the Institute of Geology and Geophysics, Chinese Academy of Sciences (IGGCAS) in Beijing, China. The trace element contents of the cassiterite samples were determined using a single collector SF-ICP-MS (Element XR, Thermo-Fisher Scientific, USA) coupled to a 193 nm ArF excimer laser (Geolas HD, Coherent, USA). The element XR instrument was equipped with a high-capacity vacuum pump (OnTool Booster 150, Asslar, Germany) that allowed for the use of a high-performance Jet sample cone. To achieve high sensitivity, helium (~0.75 L min^{-1}) was used as the carrier gas through the ablation cell and mixed with argon (0.95 L min^{-1}) downstream of the ablation cell. For the instrument details see Wu *et al.*[22,23] and Yang *et al.*[24,25] NIST SRM 612 reference materials were used for daily optimization of the instrument performance to keep the production rates of oxides

Table 1 Typical LA-(SF, MC)-ICP-MS instrument parameters for trace element and Hf isotope analyses

Laser ablation systems	Trace element analysis	Hf isotope analysis
Manufacturer, model, & type	Coherent Geolas HD	Coherent Geolas Pro
Ablation cell & volume	In-house built cell, aerosol dispersion volume <3 cm^3	Single volume ablation cell
Laser wavelength	193 nm	193 nm
Energy density/fluence	~4 J cm^{-2}	~5 J cm^{-2}
Repetition rate	5 Hz	6 Hz
Used spot size	44 μm	120 μm
Sampling mode/pattern	Single hole drilling	Single hole drilling
Ablation gas flow	~0.75 L min^{-1} (He)	~0.75 L min^{-1} (He)
Ablation duration	45 s	60 s

Instrument	SF-ICP-MS	MC-ICP-MS
Manufacturer, model, & type	Thermo-Fisher Scientific element XR	Thermo-Fisher Scientific Neptune plus
RF Power	1320 W	1350 W
Guard electrode	Connected (Pt)	Connected (Pt)
Sample cone	Nickel	Nickel Jet sample cone
Skimmer cone	Nickel	Nickel X skimmer cone
Cooling gas	15 L min^{-1}	15 L min^{-1}
Carrier gas flow (Ar)	0.95 L min^{-1}	0.95 L min^{-1}
Enhancement gas flow (N2)	none	4 mL min^{-1}
Isotopes measured (m/z) + sample time	5 ms for ^{45}Sc, ^{47}Ti, ^{90}Zr, ^{93}Nb, ^{181}Ta, 5 ms for ^{183}W and REE, 2 ms for ^{204}Pb, 10 ms for ^{208}Pb and ^{232}Th, 15 ms for ^{206}Pb and ^{238}U, 30 ms for ^{207}Pb	—
Resolution	Low (~300)	Low (~300)
Integration time	0.27 s	0.262 s

Cup configuration for Hf isotope analysis

Faraday cup	L4	L3	L2	L1	C	H1	H2	H3	H4
Mass	172	173	175	176	177	178	179	180	182
Element	Yb	Yb	Lu	Hf + Yb + Lu	Hf	Hf	Hf	Hf + W + Ta	W

(ThO^+/Th^+ < 0.5%) and double-charged ions (Ca^{2+}/Ca^+ < 1%) low.

The detailed instrument and measurement settings are summarized in Table 1. The total ablation time of 65 s included 8 s for background acquisition, 12 s for wash-out, and 45 s for data acquisition. NIST SRM 612 (ref. 26) and ARM-3 (synthetic glass)[27] were employed as reference materials for quantification of the element concentrations. The raw data (sequence of calibration materials and samples, as well as the intensities of all the isotopes in all the scans) were exported for offline data reduction using Iolite software with the "Trace_Element" DRS and the "semi quantitative" standardization method for calculation of the trace element contents.[28]

2.2 *In situ* Hf isotope determination

A Thermo-Fisher Neptune Plus MC-ICP-MS instrument (Thermo-Fisher Scientific, USA) coupled to a 193 nm ArF excimer laser ablation system was used to determine the Hf isotope ratios at IGGCAS. We adapted the method from Wu *et al.*[4] and Li *et al.*[10] for *in situ* Hf isotope measurement. The detailed instrument and measurement conditions are presented in Table 1. Prior to analysis, the instrument was tuned and optimized using Alfa Hf 14372 as the standard solution to achieve the maximum sensitivity. During the analyses, the laser fluence was set to ~5 J cm^{-2}, with the laser repetition rate and beam diameter set to 6 Hz and 120 μm, respectively. Data acquisition included 200 cycles at an integration time of 0.262 s. As there was no cassiterite reference material available for *in situ* Hf isotope analysis, we used Rond-A cassiterite as an external reference to calibrate the instrument and to monitor for mass bias drift. Two zircon reference materials, 91500 ($^{176}Hf/^{177}Hf = 0.282306 \pm 0.000008$)[29] and Mud Tank ($^{176}Hf/^{177}Hf = 0.282507 \pm 0.000006$),[30] were used for quality control and to monitor the measurement conditions. These materials were analyzed repeatedly throughout the session and yielded $^{176}Hf/^{177}Hf$ ratio of 0.282292 ± 0.000039 (2SD, $n = 43$) and 0.282492 ± 0.000032 (2SD, $n = 48$), respectively.

During *in situ* cassiterite Hf isotope analysis, isobaric interference corrections of ^{176}Yb and ^{176}Lu on ^{176}Hf have to be accurately processed. Mass bias effects for Hf were accounted for by internal normalization to $^{179}Hf/^{177}Hf = 0.7325$ (ref. 31) using the exponential law defined by:

$$R_{true} = R_{meas}\,(M_a/M_b)^{\beta} \quad (1)$$

$$\beta = \ln(R_{meas}/R_{true})/\ln(M_a/M_b) \quad (2)$$

where "R_{true}" refers to the true isotopic ratio, "R_{meas}" corresponds to the measured isotopic ratio, "M_a, M_b" are the masses of the isotopes, and "β" is the mass bias factor. The signal intensity of ^{176}Hf was calculated as:

$$^{176}Hf = {}^{176}(Hf + Lu + Yb)_{meas} - [{}^{175}Lu_{meas} \times ({}^{176}Lu/{}^{175}Lu)_{true} \times (M_{176}/M_{175})^{\beta_{Lu}} + {}^{172}Yb_{meas} \times ({}^{176}Yb/{}^{172}Yb)_{true} \times (M_{176}/M_{172})^{\beta_{Yb}}] \quad (3)$$

Compared with zircon, the $^{176}Yb/^{177}Hf$ (<0.0019) and $^{176}Lu/^{177}Hf$ (<0.0001) ratios of cassiterite are low.[11] We used the signal intensity of ^{172}Yb and ^{173}Yb and the canonical ratios of $^{172}Yb/^{173}Yb = 1.35272$ (ref. 54) to estimate the mass bias of Yb (β_{Yb}). The signal intensity of ^{175}Lu and ^{176}M and the recommended ratios of $^{176}Lu/^{175}Lu = 0.026549$ (ref. 55) were used to estimate the mass bias of Lu (β_{Lu}). The low contents of Yb and Lu (less than 1 μg g^{-1})[19,20] along with the low $^{176}Yb/^{177}Hf$ (<0.0019) and $^{176}Lu/^{177}Hf$ (<0.0001) ratios of cassiterite[11] made the obtained β_{Yb} and β_{Lu} inaccurate with large uncertainty. Therefore, we used the mass bias of Hf (β_{Hf}) to replace the mass biases of Lu (β_{Lu}) and Yb (β_{Yb}), which could not be correctly calculated due to their low signal intensity. The validity of this correction technique is discussed below. See discussion for details.

2.3 Solution Hf isotope measurement

Digestion of the cassiterite samples followed the procedure of Yang *et al.*,[18] adopted from Carr *et al.*,[32] using concentrated HBr acid. About 10 mg cassiterite powder together with 3 mL of 9 mol L^{-1} HBr were added into clean Teflon liners and kept at 210 °C in Parr autoclaves for approximately 10 days. Once the cassiterite had been digested completely, the solution was dried on a hotplate at 80 °C and then converted to nitrates by adding 1 mL of 2 mol L^{-1} HNO_3 and dried at 80 °C again. Finally, the sample residue was dissolved in 5 mL saturated boric acid in 3.5 mol L^{-1} HNO_3 at 120 °C overnight, which produced clear solutions ready for the chemical separation of Hf.

The chemical preparation of all the cassiterite samples was carried out on class 100 work benches inside a class 1000 clean laboratory. A single-step TODGA column separation was used for Hf separation adapted from Connelly *et al.*[33] An unbranched DGA Resin (Part. No., DN-B50-S, TrisKem International, France) with a particle size of 50–100 μm was used. The resin was soaked in dilute nitric acid (~2 mol L^{-1} HNO_3) prior to use. The column was washed with 5 mL 0.05 mol L^{-1} HCl, 2.5 mL 3.5 mol L^{-1} HNO_3 + 0.2 mol L^{-1} HF, 5 mL 7 mol L^{-1} HNO_3, and 10 mL Milli-Q H_2O, cleaned with 10 mL saturated boric acid in 3.5 mol L^{-1} HNO_3 before loading the sample. Once the samples were loaded onto the resin, 3.5 mol L^{-1} HNO_3 was used to effectively remove the Ti. Hf was subsequently eluted with 3.5 mol L^{-1} HNO_3 + 0.2 mol L^{-1} HF. The Hf was collected in pre-cleaned Teflon beakers and evaporated to dryness. For MC-ICP-MS measurement, the sample was taken up in 1 mL 2% HNO_3 + 0.2 mol L^{-1} HF.[34,35]

3. Results

The cassiterite samples used in this study were previously investigated for U–Pb dating and possible use as a U–Pb reference material.[18] They were collected from Neoproterozoic to Cretaceous pegmatites and tin deposits. Prior to *in situ* Hf isotope determination, the trace element contents of all the samples were determined by LA-SF-ICP-MS. The Yb/Hf and Lu/Hf ratios of these cassiterite samples are presented in Fig. 1.

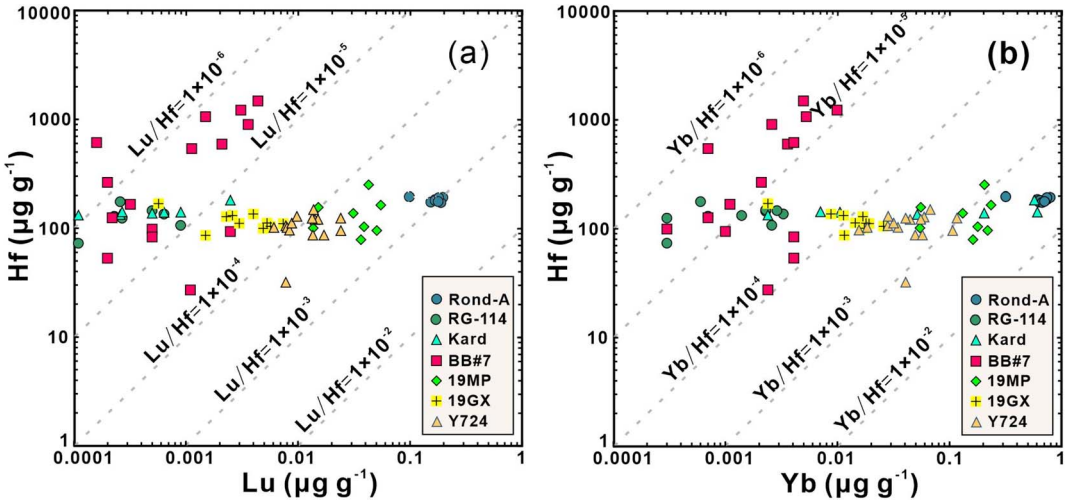

Fig. 1 Plots of the Lu/Hf ratios (a) and Yb/Hf ratios (b) of the cassiterites tested in this study. The relatively narrow range of Hf concentrations contrasted with the Lu/Hf and Yb/Hf ratios that varied by three and four orders of magnitude, respectively.

3.1 Cassiterite Rond-A (Rondônia, Brazil)

Rond-A cassiterite was collected from a placer tin deposit in the Rondônia tin province, Brazil. Previous studies determined the U–Pb age of this sample to be ~1020 Ma.[17,18] Placer cassiterite is thought to be derived from rapakivi-type granites that host polymetallic tin mineralization.[36] Debowski *et al.*[37] determined the U–Pb age and the Hf isotopic composition of zircon from 1026 Ma to 974 Ma old rapakivi granites by LA-MC-ICP-MS. Zircon yielded $^{176}Hf/^{177}Hf$ = 0.28162–0.28239, which corresponded to $\varepsilon_{Hf}(t)$ values of −15 to +11.[37]

This cassiterite sample contained an average Hf content of 184 μg g^{-1} and minor Yb and Lu contents of 0.668 and 0.170 μg g^{-1} (Table 2), respectively. The Yb/Hf and Lu/Hf ratios were relatively low and had average values of 0.0036 and 0.0009 (Fig. 1 and Table 2), respectively. *In situ* Hf isotope data suggested that Rond-A had a relatively homogeneous Hf isotopic composition with average values of $^{176}Hf/^{177}Hf$ = 0.28217 ± 0.00008 (2SD, n = 59; Fig. 2a) and $\varepsilon_{Hf}(t)$ = + 0.88 ± 2.73 (2SD, n = 59; Fig. 2b). These values were in good agreement with the values determined from solutions. Three separate aliquots of Rond-A analyzed by MC-ICP-MS gave $^{176}Hf/^{177}Hf$ = 0.28217 ± 0.00003 (2SD, n = 3; Fig. 2a) and $\varepsilon_{Hf}(t)$ = + 0.97 ± 1.13 (2SD, n = 3; Fig. 2b), respectively. The *in situ* and solution-based results were identical and fell in the range known for zircon from local polymetallic tin mineralization.[37]

Table 2 Average trace element contents of the cassiterite samples as determined by LA-SF-ICP-MS[b]

Sample	Rond-A	RG-114	Kard	BB#7	19MP	19GX	Y724
n[a]	10	10	7	15	8	10	16
Unit	μg g^{-1}	μg g^{-1}	μg g^{-1}	μg g^{-1}	μg g^{-1}	μg g^{-1}	μg g^{-1}
Sc	294	7.0	1.5	4.8	64	5.4	262
Ti	715	3119	2561	2200	377	8648	6551
Zr	643	575	426	2451	688	870	791
Nb	9577	7992	176	28039	2001	53	3055
Yb	0.668	0.002	0.212	0.003	0.157	0.064	0.050
Lu	0.170	0.001	0.028	0.002	0.035	0.016	0.013
Hf	184	132	145	489	137	120	108
Ta	8889	4220	1037	16383	767	4	950
W	99	103	18	116	3815	1720	5346
Pb	0.05	0.03	0.87	0.18	0.26	0.02	0.86
Th	0.036	0.003	0.073	0.003	0.006	0.010	0.254
U	3.2	2.2	1.7	23	21	21	222
HFSE	20008	16038	4345	49561	3970	9695	11454
Yb/Hf	0.0036	<0.0001	0.0015	<0.0001	0.0012	0.0005	0.0005
Lu/Hf	0.0009	<0.0001	0.0002	<0.0001	0.0003	0.0001	0.0001

[a] "n" represents the number of analyses. [b] Some Yb/Hf and Lu/Hf ratios are extremely low, which might be one or two orders of magnitude smaller than 0.0001. Individual analyses of the trace elements are given in ESI Table 1.

3.2 Cassiterite RG-114 (Kalima, Democratic Republic of the Congo)

Cassiterite sample RG-114 was collected from a quartz vein of the Kalima area, Maniema province, Democratic Republic of the Congo. The emplacement of the quartz veins altered the Kalima granite and adjacent Mesoproterozoic metasedimentary rocks.[38] Yang *et al.*[18] reported LA-SF-ICP-MS and ID-TIMS U-Pb ages of ~1020 Ma for RG-114 cassiterite. There are no Hf isotope data available for whole rock or zircon samples from this area.

RG-114 had moderate Hf contents with an average value of 132 μg g^{-1} and Yb and Lu contents of less than 0.002 μg g^{-1} (Table 2). The Yb/Hf and Lu/Hf ratios were extremely low (<0.0001; Fig. 1 and Table 2). *In situ* Hf isotope analysis revealed that the Hf isotopic compositions of RG-114 cassiterite were strongly heterogeneous (Fig. 2c and d) with LA-MC-ICP-MS $^{176}Hf/^{177}Hf$ ratios and $\varepsilon_{Hf}(t)$ values ranging from 0.28172 ± 0.00011 to 0.28217 ± 0.00010 and from −14.55 ± 4.10 to −0.04 ± 3.27, respectively. The average values for the *in situ* data agreed well with the solution-based results of 0.28189 ± 0.00003 (2SD, n = 3; Fig. 2c) and −8.77 ± 1.09 (2SD, n = 3; Fig. 2d) using larger sample volumes.

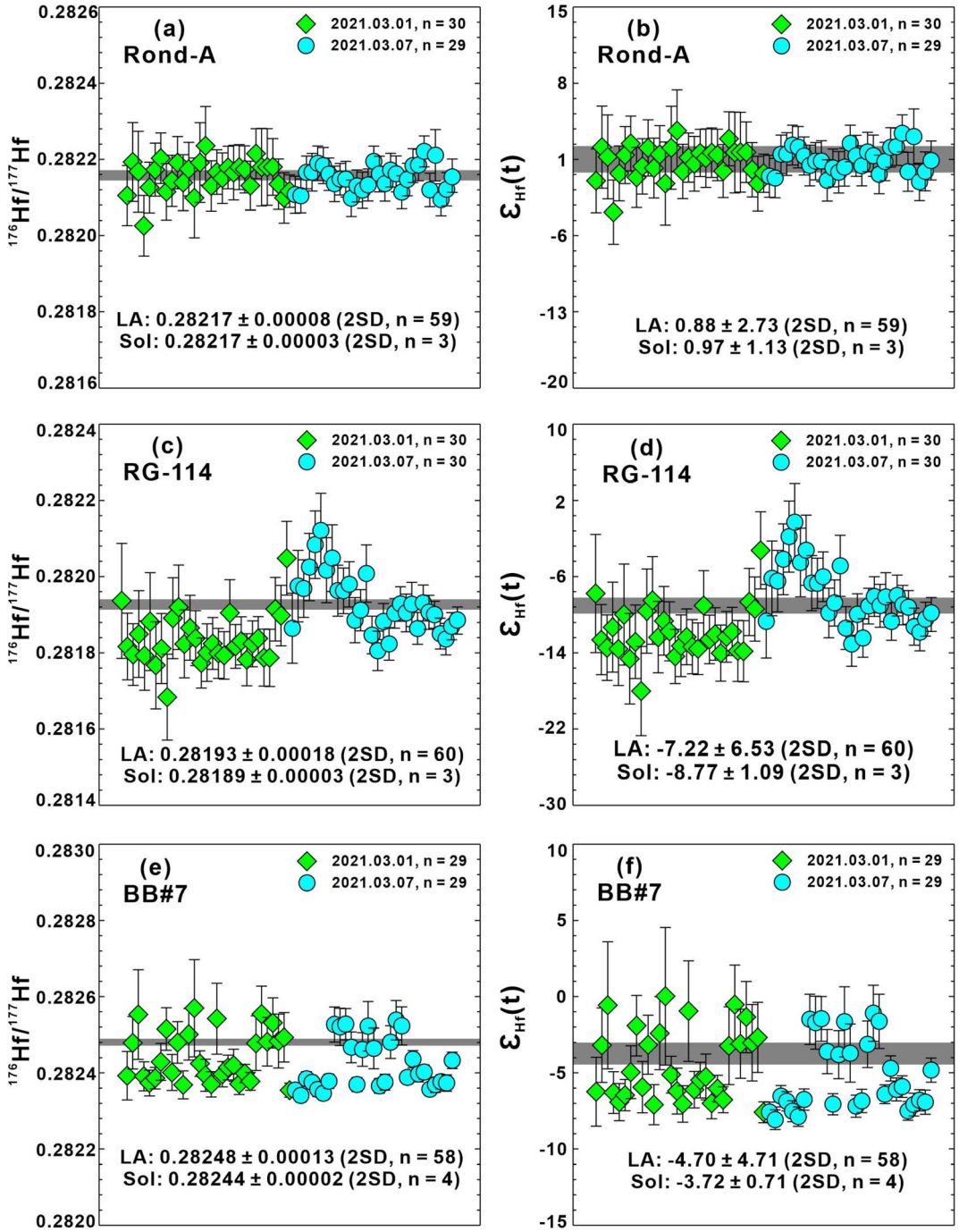

Fig. 2 $^{176}Hf/^{177}Hf$ ratios and $\varepsilon_{Hf}(t)$ values of Rond-A (a and b), RG-114 (c and d), and BB#7 (e and f) cassiterite. The green diamond and blue circle symbols represent the results obtained by laser ablation. The dark band represents the solution results and their uncertainties.

3.3 Cassiterite BB#7 (Oxford County, Maine, USA)

BB#7 was sampled from a zoned lithium–caesium–tantalum (LCT) type pegmatite in the BB#7 pegmatite quarry, Oxford County, Maine, USA. An age of ~262 Ma was obtained for this sample using U–Pb LA-SF-ICP-MS and ID-TIMS dating.[18] Fu *et al.*[39] analyzed the zircon from a muscovite granite that seemed to be genetically related with the pegmatite,[40,41] obtaining LA-MC-ICP-MS $^{176}Hf/^{177}Hf$ ratios ranging from 0.28243 to 0.28257, corresponding to $\varepsilon_{Hf}(t)$ values of −5.2 to +2.1.

BB#7 had the highest Hf content among the investigated samples and also showed the largest variation. The average Hf, Yb, and Lu contents were 489, 0.003, and 0.002 μg g^{-1} (Table 2),

respectively. The Yb/Hf and Lu/Hf ratios were below 0.0001 (Fig. 1 and Table 2). *In situ* Hf isotope analysis revealed that BB#7 showed some variation with $^{176}Hf/^{177}Hf$ ratios ranging from 0.28239 ± 0.00002 to 0.28259 ± 0.00005 and the corresponding $\varepsilon_{Hf}(t)$ values ranging from −7.80 ± 0.65 to −0.02 ± 4.51 (Fig. 2e and f). Individual analyses of BB#7 obtained by LA-MC-ICP-MS revealed that the laser ablation results possibly fell in two groups. Analyses of the group with the lower $^{176}Hf/^{177}Hf$ ratios generally did not overlap within uncertainties with the solution-based average $^{176}Hf/^{177}Hf$ ratio of 0.28244 ± 0.00002 (2SD, $n = 4$; Fig. 2e) and the $\varepsilon_{Hf}(t)$ value of −3.72 ± 0.71 (2SD, $n = 4$; Fig. 2f). The laser ablation and solution $^{176}Hf/^{177}Hf$ ratios were slightly lower than those of zircon from the nearby granite.[39]

3.4 Cassiterite Kard (Kekekaerde, East Kunlun Orogen, China)

This sample was collected from the Kekekaerde W–Sn deposit in the Baiganhu W–Sn ore field, East Kunlun Orogen, NW China. Tin mineralization of this deposit mainly occurs in quartz veins and greisens.[42–45] Yang *et al.*[18] reported the U–Pb age of Kard cassiterite as 429.1 ± 6.4 Ma. Zircon from granite related to the mineralization yielded LA-MC-ICP-MS $^{176}Hf/^{177}Hf$ ratios ranging from 0.282447 to 0.282571 by Gao *et al.*[46]

The cassiterite sample Kard had Hf, Yb, and Lu contents of 145, 0.212, and 0.028 μg g^{-1} (Table 2), respectively. The Yb/Hf and Lu/Hf ratios were 0.0015 and 0.0002 (Fig. 1 and Table 2). Cassiterite Kard had a relatively homogeneous Hf isotopic composition with an average LA-MC-ICP-MS $^{176}Hf/^{177}Hf$ ratio of 0.28246 ± 0.00008 (2SD, $n = 60$; Fig. 3a) and a corresponding $\varepsilon_{Hf}(t)$ value of −1.84 ± 2.75 (2SD, $n = 60$; Fig. 3b). Due to the limited amount of sample available, Kard was not analyzed by the solution MC-ICP-MS technique. The $^{176}Hf/^{177}Hf$ ratios obtained by laser ablation for cassiterite and the solution method for zircon from the same deposit[46] were identical.

3.5 Cassiterite 19MP (Maoping, Jiangxi Province, China)

Cassiterite sample 19MP was collected from Maoping W–Sn deposit, Jiangxi Province, China. Previous studies constrained the age of Maoping rare metal granite to be 155–150 Ma.[47] Yang *et al.*[18] measured the U–Pb age of cassiterite 19MP to be 156.3 ± 2.4 Ma (unpublished data). The zircon $^{176}Hf/^{177}Hf$ ratios ranged from 0.282344 to 0.282575 with corresponding $\varepsilon_{Hf}(t)$ values of

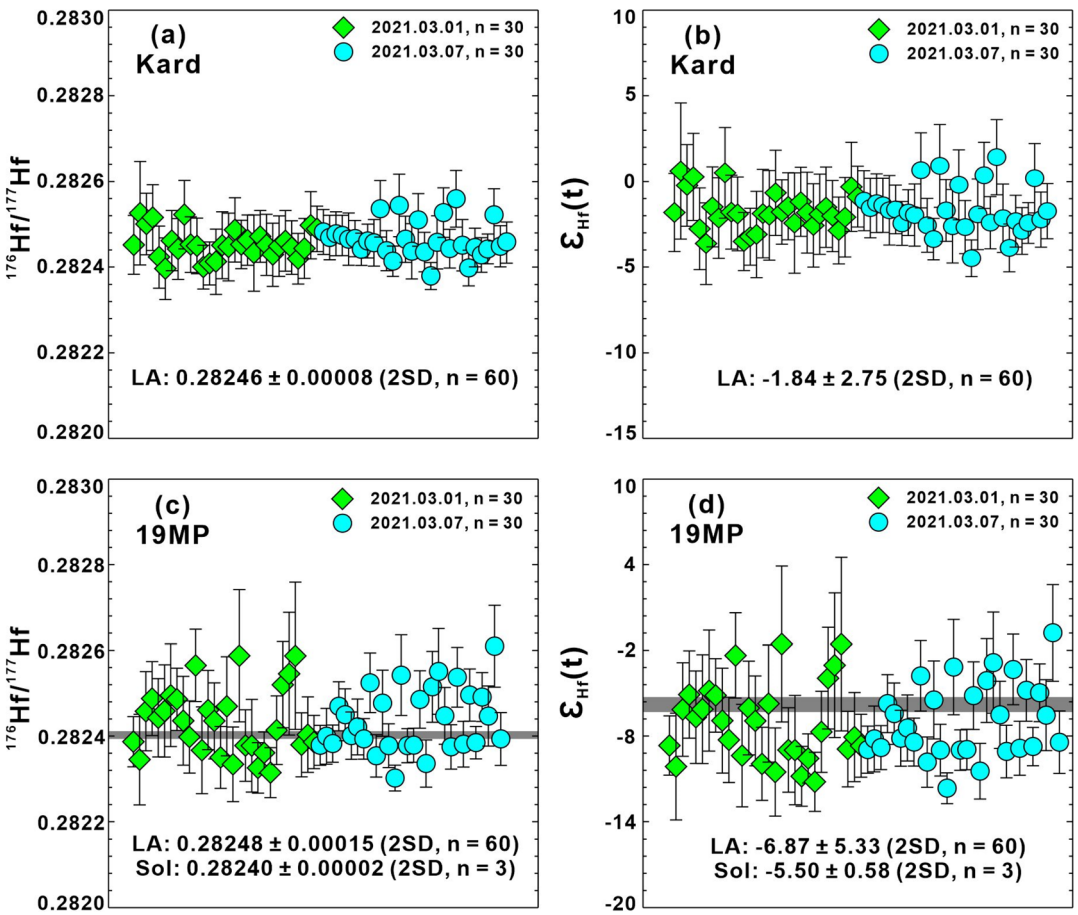

Fig. 3 $^{176}Hf/^{177}Hf$ ratios and $\varepsilon_{Hf}(t)$ values of the cassiterite samples Kard (a and b) and 19MP (c and d). The green diamond and blue circle symbols represent the laser ablation results, whereas the dark line shows the solution result and its uncertainty.

−11.8 to −3.5,[48] which differed slightly from the whole rock data ($^{176}Hf/^{177}Hf$ ratios: 0.282365–0.282698; $\varepsilon_{Hf}(t)$ values: −16.3 to −7.4 (ref. 49)).

Cassiterite 19MP had a Hf mass fraction of 137 μg g^{-1} (Table 2) and contained small amounts of Yb (0.157 μg g^{-1}) and Lu (0.035 μg g^{-1}). The Yb/Hf and Lu/Hf ratios were 0.0012 and 0.0003 (Fig. 1 and Table 2). Individual LA-MC-ICP-MS *in situ* Hf isotope analyses of 19MP showed a relatively large variation (Fig. 3c and d) with $^{176}Hf/^{177}Hf$ ratios ranging from 0.28235 ± 0.00006 to 0.28266 ± 0.00010 and corresponding $\varepsilon_{Hf}(t)$ values ranging from −11.37 ± 1.08 to −0.49 ± 3.38. The average solution-based $^{176}Hf/^{177}Hf$ and $\varepsilon_{Hf}(t)$ values were 0.28240 ± 0.00002 (2SD, $n = 60$; Fig. 3c) and −5.50 ± 0.58 (2SD, $n = 60$; Fig. 3d), respectively. The results for cassiterite acquired by the *in situ* and solution methods were identical within uncertainties and agreed well with the values reported for the associated granite.[48,49]

3.6 Cassiterite 19GX (Shanhu W–Sn deposit, Guangxi Province, China)

Cassiterite sample 19GX was collected from the Shanhu W–Sn deposit, Guangxi Province, China. This sample was dated by both ID-TIMS and LA-SF-ICP-MS techniques with an age of ~100 Ma.[18] Zhang *et al.*[50] reported the U–Pb zircon age of the Yantianling muscovite granite (W–Sn mineralization related) to be ~100 Ma and the Hf $^{176}Hf/^{177}Hf$ ratios and $\varepsilon_{Hf}(t)$ values of zircon to range from 0.282349 to 0.282464 and from −12.7 to −7.8, respectively.

Cassiterite 19GX has Hf, Yb, and Lu contents of 120, 0.064, and 0.016 μg g^{-1} (Table 2), respectively. Both Yb/Hf and Lu/Hf ratios are below 0.0001 (Fig. 1 and Table 2). Cassiterite 19GX showed some variation in its Hf isotopic composition with LA-MC-ICP-MS analyses indicating $^{176}Hf/^{177}Hf$ ratios ranging from 0.28241 ± 0.00010 to 0.28276 ± 0.00009, and $\varepsilon_{Hf}(t)$ values ranging from −10.58 ± 3.67 to +1.85 ± 3.05 (Fig. 4a and b). The average $^{176}Hf/^{177}Hf$ ratio and $\varepsilon_{Hf}(t)$ value measured by the solution-based method were 0.28249 ± 0.00001 (2SD, $n = 3$; Fig. 4a) and −7.20 ± 0.97 (2SD, $n = 3$; Fig. 4b), respectively, which were slightly lower than the values obtained by laser ablation. The solution results agreed within uncertainties with the values of zircon separated from the Yantianling granite,[50] whereas the cassiterite values obtained by the laser ablation were slightly higher than the zircon values.[50]

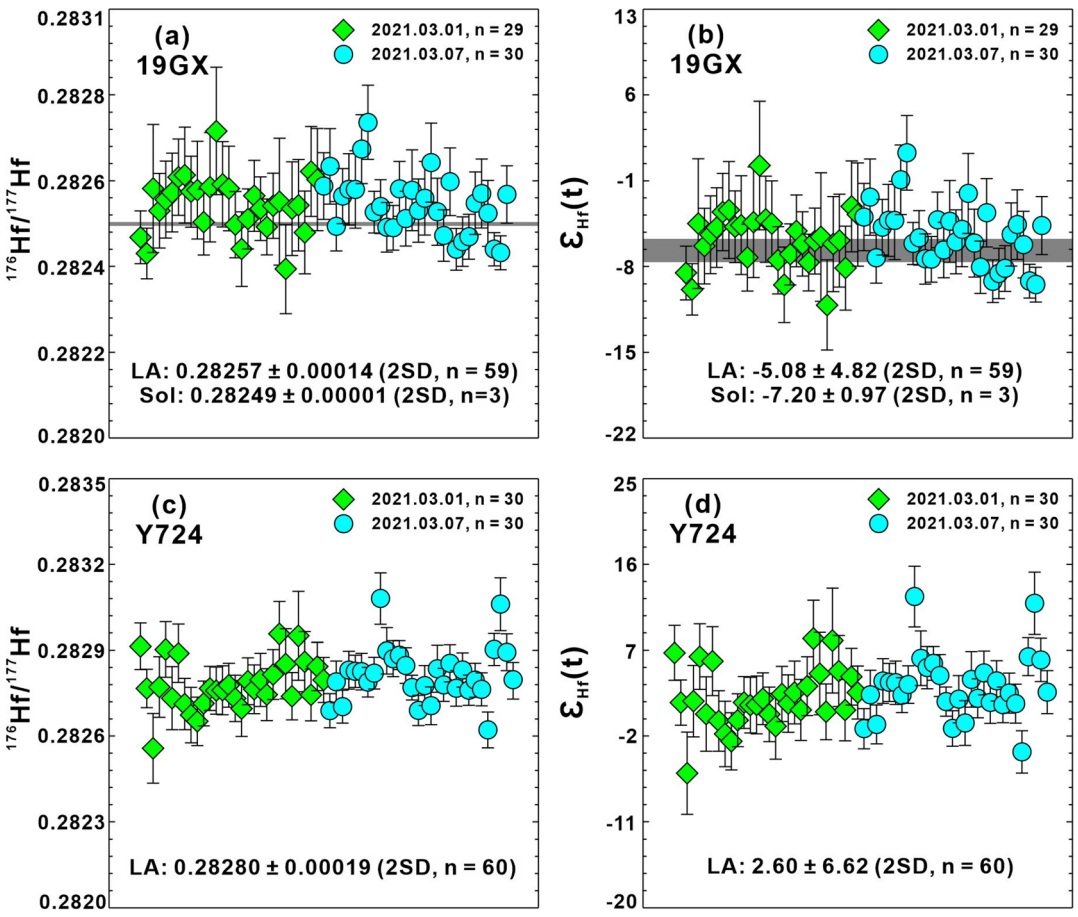

Fig. 4 $^{176}Hf/^{177}Hf$ ratios and $\varepsilon_{Hf}(t)$ values of 19GX (a and b) and Y724 (c and d). The green diamond and blue circle symbols represent the laser ablation results, whereas the dark line and its width show the solution results and their uncertainty.

3.7 Cassiterite Y724 (Yinyan porphyry tin deposit, Guangdong Province, China)

Cassiterite Y724 was sampled from the Yinyan porphyry tin deposit that is temporally and spatially associated with the Xishan A-type granite, Guangdong Province, China.[51,52] Hu *et al.*[52] and Yang *et al.*[18] reported the U–Pb age of Y724 cassiterite to be 78.2 ± 0.7 Ma and 78.3 ± 0.9 Ma, respectively. Zheng *et al.*[53] characterized the Hf isotopic composition of the Xishan A-type granite close to the sample location of the cassiterite sample to range from 0.282455 to 0.282725 for $^{176}Hf/^{177}Hf$ ratios and −9.6 to −0.1 for $\varepsilon_{Hf}(t)$ values.

Cassiterite sample Y724 had the lowest average Hf content (108 μg g^{-1} Table 2) among the cassiterite samples investigated here and had extremely low Yb/Hf (0.0005) and Lu/Hf (0.0001) ratios (Fig. 1 and Table 2). The *in situ* Hf isotope ratios of cassiterite Y724 were scattered and fall in the 0.28262 ± 0.00006 to 0.28308 ± 0.00009 ranges for $^{176}Hf/^{177}Hf$ ratios and −5.90 ± 4.32 to + 12.61 ± 3.18 for $\varepsilon_{Hf}(t)$ values (Fig. 4c and d). Cassiterite Y724 was not analyzed using the solution-based MC-ICP-MS technique. Despite the large variation in Hf isotopic composition in Y724 cassiterite, our $^{176}Hf/^{177}Hf$ ratios were much higher than those of zircon.[53]

4. Discussion

4.1 Isobaric interferences

In situ Hf isotope measurement is hampered by interferences from ^{176}Yb and ^{176}Lu on the ^{176}Hf signal. These isobaric interferences can be corrected using ^{173}Yb and ^{175}Lu and the natural $^{172}Yb/^{173}Yb$ and $^{176}Lu/^{175}Lu$ ratios.[4,5,56–58] The Yb/Hf and Lu/Hf ratios of cassiterite typically are very low (Fig. 1). For instance, Kendall-Langley *et al.*[11] reported extremely low $^{176}Yb/^{177}Hf$ and $^{176}Lu/^{177}Hf$ ratios of <0.0019 and <0.0001 for cassiterite from Western Australia. Such values are several orders of magnitude lower than those of igneous zircon and can barely affect the final results. Fig. 5 illustrates the effect of the isobaric interferences of ^{176}Yb and ^{176}Lu on $^{176}Hf/^{177}Hf$ for cassiterite Rond-A, which had the highest $^{176}Yb/^{177}Hf$ ratios of the analyzed cassiterite samples. The maximum deviation of the $^{176}Hf/^{177}Hf$ ratios was about 60 ppm for cassiterite Rond-A. For comparison, the effect was near 20 ppm for cassiterite BB#7, which had the lowest $^{176}Yb/^{177}Hf$ ratio. This indicates that the $^{176}Yb/^{177}Hf$ ratios have a marked effect on the $^{176}Hf/^{177}Hf$ ratios measurements.

We evaluated the effect of Yb correction on obtaining the accurate Hf isotopic composition. Sample Rond-A was used as an example, because it had the highest Yb content among the investigated samples. As shown in Fig. 7a, the $^{176}Hf/^{177}Hf$ ratios without Yb correction (dark green diamonds) were much higher than that for the data with Yb correction (green diamonds), which was mainly caused by the contribution of ^{176}Yb and ^{176}Lu. Therefore, Yb correction is necessary during *in situ* cassiterite Hf isotope analysis. The decay of ^{176}Lu produces ^{176}Hf. The ~1020 Ma old cassiterite Rond-A had a $^{176}Lu/^{177}Hf$ ratio of less than 0.001, which implied that *in situ* ^{176}Hf growth increased the $^{176}Hf/^{177}Hf$ ratio by 0.00002 only. In the context of the analytical precision, such a small shift does not affect the measured $^{176}Hf/^{177}Hf$ ratio. The other analyzed cassiterite samples had lower $^{176}Lu/^{177}Hf$ ratios or were younger, which implied that the effect of *in situ* ^{176}Hf growth was even smaller.

4.2 Matrix effects between zircon and cassiterite

Unlike for solution-based Hf isotope analysis, a matrix-matched reference material is critical to obtain accurate results for *in situ* Hf isotope measurements. The lack of a matrix-matched reference material is the main limitation for the *in situ* Hf isotope analysis of cassiterite. To further evaluate the influence of matrix effects, we employed cassiterite Rond-A, which was characterized by the most homogeneous Hf isotope composition among the analyzed samples, as the external calibration

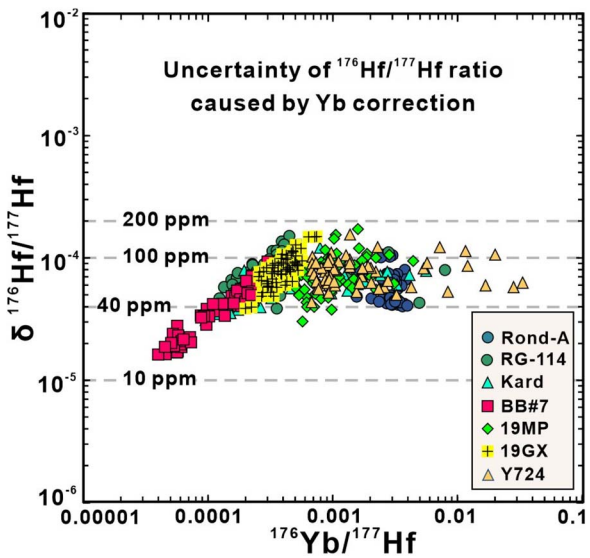

Fig. 5 Uncertainty of the $^{176}Hf/^{177}Hf$ ratio caused by Yb correction.

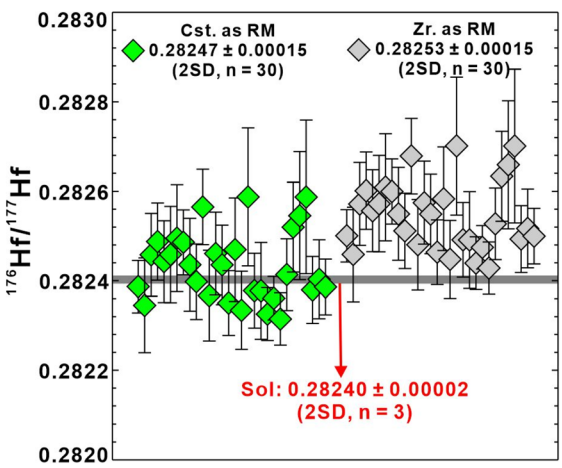

Fig. 6 $^{176}Hf/^{177}Hf$ ratio of 19MP calibrated against cassiterite Rond-A (green diamond) and zircon Mud Tank (grey diamond), respectively. Abbreviation: Cst., cassiterite; Zr., zircon; RM, reference material; Sol, solution-based method.

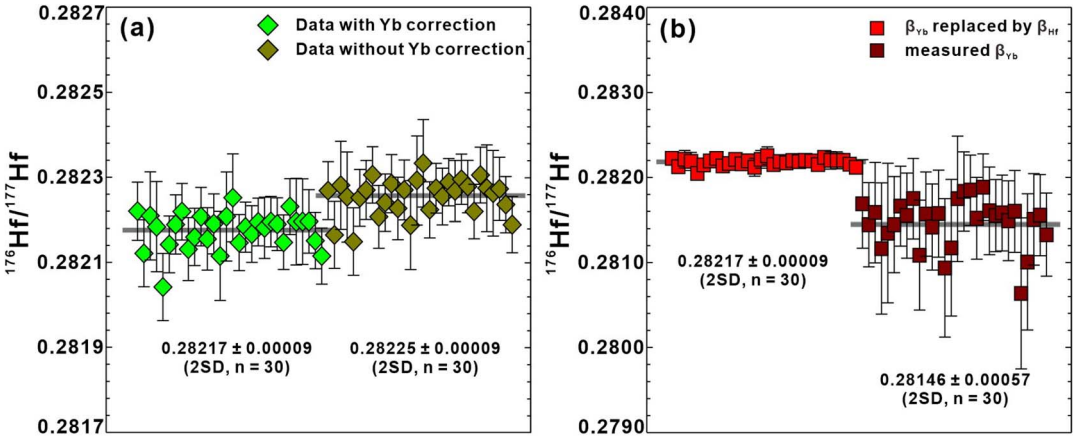

Fig. 7 Effect of Yb isobaric interference on the determination of accurate $^{176}Hf/^{177}Hf$ ratios. (a) $^{176}Hf/^{177}Hf$ ratios with (green diamonds) and without (dark green diamonds) Yb correction. (b) Comparison of the β_{Hf} (red squares) and β_{Yb} (dark red squares) correction. All the data were from cassiterite sample Rond-A.

reference material to calculate the Hf isotope ratios of other cassiterite samples. The matrix effect was illustrated for cassiterite 19MP (Fig. 6), which was analyzed using cassiterite Rond-A and zircon Mud Tank as the external calibration reference material. The $^{176}Hf/^{177}Hf$ ratios of 19MP calibrated against cassiterite (green diamond) agreed well with the solution-based ratios. In contrast, the $^{176}Hf/^{177}Hf$ ratios of 19MP calibrated against zircon (grey diamonds) had much higher values. This indicated that there was a strong matrix effect between zircon and cassiterite during laser ablation.

4.3 Accurate Hf isotope measurement of cassiterite by LA-MC-ICP-MS

The good agreement of the $^{176}Hf/^{177}Hf$ ratios measured by LA-MC-ICP-MS with the solution-based MC-ICP-MS values for the cassiterite samples demonstrated that Hf isotopes can be measured accurately for cassiterite with ≥100 μg g^{-1} Hf using the technique used here. Individual measurements of $^{176}Hf/^{177}Hf$ showed relatively large uncertainties due to the low Hf content (typically ± 3–4 ε_{Hf} unit for samples with 100 μg g^{-1} Hf). The precision obtained for cassiterite was much poorer than for zircon, but it was still sufficient to distinguish the $^{176}Hf/^{177}Hf$ values of different cassiterite samples. The obtained Hf isotopic compositions of the investigated cassiterite samples were in good agreement with the zircon data from associated granites.

The data reduction scheme was adapted from Li *et al.*[10] who established the protocol for *in situ* rutile Hf isotope measurement. The low Yb and Lu contents hamper the calculation of the mass bias of Yb (β_{Yb}) and Lu (β_{Lu}) due to their low signal intensity. This is illustrated in Fig. 7b for cassiterite sample Rond-A, which had the highest Yb contents of the cassiterite samples studied. Because of the low contents of Yb in cassiterite, the uncertainty of β_{Yb} was large and may result in an

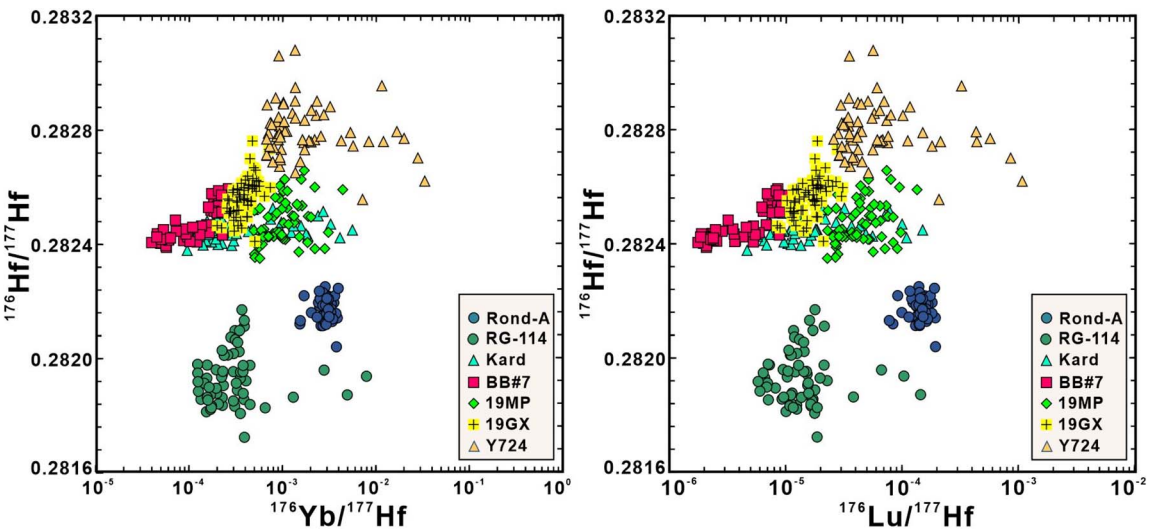

Fig. 8 Comparison of the $^{176}Hf/^{177}Hf$, $^{176}Yb/^{177}Hf$, and $^{176}Lu/^{177}Hf$ ratios of the analyzed cassiterite samples.

Table 3 *In situ* Hf isotope ratios determined by LA-MC-ICP-MS

Cassiterite	n^a	$^{178}Hf^b$ (V)	$^{176}Yb/^{177}Hf$	2SD	$^{176}Lu/^{177}Hf$	2SD	$^{176}Hf/^{177}Hf$	2SD	$\varepsilon_{Hf}(t)$	2SD
Rond-A (~1020 Ma)										
2021.03.01	30	0.24	0.00289	0.00099	0.00015	0.00005	0.28217	0.00009	0.88	3.04
2021.03.07	29	0.46	0.00302	0.00099	0.00014	0.00005	0.28217	0.00007	0.88	2.43
Mean	59	0.35	0.00295	0.00099	0.00014	0.00005	0.28217	0.00008	0.88	2.73
RG-114 (~1020 Ma)										
2021.03.01	30	0.22	0.00067	0.00293	0.00002	0.00004	0.28188	0.00014	−9.11	4.97
2021.03.07	30	0.35	0.00041	0.00173	0.00002	0.00005	0.28198	0.00016	−5.32	5.70
Mean	60	0.29	0.00054	0.00240	0.00002	0.00004	0.28193	0.00018	−7.22	6.53
Kard (~430 Ma)										
2021.03.01	30	0.26	0.00097	0.00271	0.00003	0.00007	0.28245	0.00007	−2.07	2.47
2021.03.07	30	0.41	0.00039	0.00088	0.00001	0.00002	0.28247	0.00008	−1.61	2.98
Mean	60	0.34	0.00068	0.00208	0.00002	0.00005	0.28246	0.00008	−1.84	2.75
BB#7 (~262 Ma)										
2021.03.01	29	0.48	0.00018	0.00023	0.00001	0.00001	0.28249	0.00013	−4.35	4.62
2021.03.07	29	1.19	0.00011	0.00015	0.00000	0.00001	0.28247	0.00013	−5.05	4.77
Mean	58	0.84	0.00014	0.00021	0.00001	0.00001	0.28248	0.00013	−4.70	4.71
19MP (~155 Ma)										
2021.03.01	30	0.21	0.00113	0.00100	0.00005	0.00003	0.28247	0.00015	−7.10	5.48
2021.03.07	30	0.36	0.00120	0.00174	0.00005	0.00005	0.28249	0.00015	−6.63	5.22
Mean	60	0.28	0.00117	0.00141	0.00005	0.00004	0.28248	0.00015	−6.87	5.33
19GX (~100 Ma)										
2021.03.01	29	0.19	0.00041	0.00026	0.00002	0.00001	0.28256	0.00013	−5.25	4.68
2021.03.07	30	0.29	0.00040	0.00019	0.00002	0.00001	0.28257	0.00014	−4.92	5.02
Mean	59	0.24	0.00040	0.00022	0.00002	0.00001	0.28257	0.00014	−5.08	4.82
Y724 (~78 Ma)										
2021.03.01	30	0.20	0.00306	0.00877	0.00010	0.00025	0.28278	0.00018	1.97	6.25
2021.03.07	30	0.31	0.00415	0.01584	0.00013	0.00048	0.28281	0.00019	3.22	6.85
Mean	60	0.25	0.00360	0.01274	0.00011	0.00038	0.28280	0.00019	2.60	6.62

[a] "n" represents the number of analyses. [b] "V" represents the signal intensity. The reading of 1 V corresponds to ~9.0×10^5 cps.

overcorrection of the $^{176}Hf/^{177}Hf$ ratios. This was indicated by the large uncertainties of the β_{Yb}-corrected $^{176}Hf/^{177}Hf$ ratio (0.281146 ± 0.00057, 2SD, $n = 30$; Fig. 7b), which was lower than the solution-based value. In contrast, the data corrected using β_{Hf} yielded an average $^{176}Hf/^{177}Hf$ ratio of 0.28217 ± 0.00009 (2SD, $n = 30$; Fig. 7b) and agreed well with the solution-based result, which verified the feasibility of our method.

Despite the variable Hf isotope composition in some cassiterite samples, the $^{176}Hf/^{177}Hf$ ratios determined by laser ablation agreed within uncertainty with their solution-based data. This suggests that the variation in the Hf isotope composition was mainly caused by inhomogeneity of the sample themselves.

4.4 Potential cassiterite reference materials for *in situ* Hf isotope analysis

A standard reference material is needed to calibrate the instrument and monitor for mass drift during *in situ* Hf analysis by LA-MC-ICP-MS. In contrast to the well-established *in situ* zircon Hf isotope method, there are presently no cassiterite reference materials. During the course of this study, we used cassiterite sample Rond-A as a reference material. The long-term *in situ* $^{176}Hf/^{177}Hf$, $^{176}Lu/^{177}Hf$, and $^{176}Yb/^{177}Hf$ values of Rond-A were homogeneous (Fig. 8). The laser ablation (0.28217 ± 0.00008, 2SD, $n = 59$; Table 3) and solution-based (0.28217 ± 0.00003, 2SD, $n = 3$; Table 4) $^{176}Hf/^{177}Hf$ ratios agreed. Therefore, Rond-A is suitable as standard reference material for *in situ* cassiterite Hf isotope determination beyond this study.

Among the investigated cassiterite samples, RG-114 and Y724 showed the largest variation in $^{176}Hf/^{177}Hf$ and cannot be used as reference materials. Samples BB#7, 19MP, and 19GX also showed some variation in $^{176}Hf/^{177}Hf$. As the laser ablation and the solution-based results were in good agreement, these samples possibly may serve as secondary reference materials. Sample Kard had homogeneous $^{176}Hf/^{177}Hf$ ratios and could serve as a reference material once its $^{176}Hf/^{177}Hf$ ratio has been determined by the solution-based method. Materials RG-114, BB#7, 19MP, and 19GX are available upon request to other laboratories. Materials Rond-A, Kard, and Y724 originally were introduced by other groups[17,45,52] and, therefore, we have only limited amounts available for distribution to other laboratories.

Table 4 Hf isotopic data of the cassiterite samples obtained by the solution-based method

Cassiterite	$^{176}Hf/^{177}Hf$	2SE	$\varepsilon_{Hf}(t)^a$
Rond-A (~1020 Ma)			
1	0.282192	0.000008	1.62
2	0.282166	0.000008	0.69
3	0.282163	0.000011	0.60
Mean	0.282174		0.97
2SD	0.000032		1.13
RG-114 (~1020 Ma)			
1	0.281903	0.000010	−8.17
2	0.281895	0.000012	−8.45
3	0.281875	0.000010	−9.15
4	0.281871	0.000010	−9.30
Mean	0.281886		−8.77
2SD	0.000031		1.09
BB#7 (~262 Ma)			
1	0.282518	0.000015	−3.28
2	0.282504	0.000017	−3.78
3	0.282507	0.000017	−3.66
4	0.282493	0.000016	−4.14
Mean	0.282505		−3.72
2SD	0.000020		0.71
19MP (~155 Ma)			
1	0.282508	0.000015	−5.83
2	0.282524	0.000016	−5.26
3	0.282520	0.000015	−5.42
Mean	0.282517		−5.50
2SD	0.000017		0.58
19GX (~100 Ma)			
1	0.282491	0.000014	−7.73
2	0.282518	0.000013	−6.78
3	0.282509	0.000016	−7.09
Mean	0.282506		−7.20
2SD	0.000027		0.97

[a] $\varepsilon_{Hf}(t)$ are calculated from the measured $^{176}Hf/^{177}Hf$ ratios and the age of the samples. The samples have very low $^{176}Lu/^{177}Hf$ ratios and therefore the contributions from the *in situ* growth of ^{176}Hf are insignificant.

5. Conclusions

A matrix-matched reference material is crucial to obtain precise and accurate Hf isotope data by LA-MC-ICP-MS. Our *in situ* cassiterite Hf isotope results were consistent within uncertainties with solution-based MC-ICP-MS measurements on aliquots from the same samples or with published results for the same tin deposit. Our results indicated the feasibility of the established analytical protocol for *in situ* cassiterite Hf isotope analysis. The interferences of Yb and Lu in cassiterite affected the measured $^{176}Hf/^{177}Hf$ ratios. Hence, Yb correction was necessary in order to obtain reasonable data.

Cassiterite samples Rond-A and Kard showed homogeneous Hf isotopic compositions. We recommend cassiterite Rond-A for use as a primary reference material for *in situ* Hf isotope analysis. Cassiterite Kard is also suitable as a primary reference material once its Hf isotopic composition has been determined by solution-based MC-ICP-MS. Cassiterite samples BB#7, 19MP, and 19GX showed some variation in their Hf isotopic composition, but may possibly be used as secondary reference materials.

Data availability

The data that support the findings of this study are available in the online ESI† of this article.

Author contributions

Conceptualization, M. Y. and Y.-H. Y.; investigation, M. Y.; formal analysis, M. Y.; methodology, Y.-H. Y.; supervision, Y.-H. Y. and R.-L. R.; writing – original draft, M. Y.; writing – review & editing, R.-L. R., S.-T. W, T. W. and H. W.; funding acquisition, Y.-H. Y.

Conflicts of interest

The authors declare no conflict of interest.

Acknowledgements

This work was financially supported by National Natural Science Foundation of China (Grants 42173034). We are indebted to Leonid A. Neymark (Rond-A), Fu-Yuan Wu (RG-114), Ting-Guang Lan (Kard), Xiao-Feng Li (19MP and 19GX), Hong Zhong (Y724), and Tony Nikischer (BB#7) for providing cassiterite samples.

References

1 P. J. Patchett, *Geochim. Cosmochim. Acta*, 1983, **47**, 81–91.
2 Y. Amelin, D. C. Lee, A. N. Halliday and R. T. Pidgeon, *Nature*, 1999, **399**, 252–255.
3 J. D. Woodhead, J. M. Hergt, J. P. Davidson and S. M. Eggins, *Earth Planet. Sci. Lett.*, 2001, **192**, 331–346.
4 F. Y. Wu, Y. H. Yang, L. W. Xie, J. H. Yang and P. Xu, *Chem. Geol.*, 2006, **234**, 105–126.
5 M. F. Thirlwall and A. J. Walder, *Chem. Geol.*, 1995, **122**, 241–247.
6 T. M. Harrison, J. Blichert-Toft, W. Muller, F. Albarede, P. Holden and S. J. Mojzsis, *Science*, 2005, **310**, 1947–1950.
7 C. J. Hawkesworth and A. I. S. Kemp, *Chem. Geol.*, 2006, **226**, 144–162.
8 A. I. S. Kemp, C. J. Hawkesworth, B. A. Paterson and P. D. Kinny, *Nature*, 2006, **439**, 580–583.
9 T. A. Ewing, D. Rubatto, S. M. Eggins and J. Hermann, *Chem. Geol.*, 2011, **281**, 72–82.
10 Y. Li, Y. H. Yang, S. J. Jiao, F. Y. Wu, J. H. Yang and L. W. Xie, *Sci. China: Earth Sci.*, 2015, **58**, 2134–2144.
11 L. A. Kendall-Langley, A. I. S. Kemp, J. L. Grigson and J. Hammerli, *Lithos*, 2020, **352–353**, 105231.
12 Z. M. Tang, X. D. Che, Y. H. Yang, F. Y. Wu, R. C. Wang, J. H. Yang, A. Gerdes, Z. Y. Zhu, F. Liu and C. Zhang, *J. Anal. At. Spectrom.*, 2021, **36**, 1643–1656.

13 B. L. Gulson and M. T. Jones, *Geology*, 1992, **20**, 355–358.
14 S. D. Yuan, J. T. Peng, R. Z. Hu, H. M. Li, N. P. Shen and D. L. Zhang, *Miner. Deposita*, 2008, **43**, 375–382.
15 S. D. Yuan, J. T. Peng, S. Hao, H. M. Li, J. Z. Geng and D. L. Zhang, *Ore Geol. Rev.*, 2011, **43**, 235–242.
16 P. A. Carr, M. D. Norman and V. C. Bennett, *Chem. Geol.*, 2017, **467**, 122–133.
17 L. A. Neymark, C. S. Holm-Denoma and R. J. Moscati, *Chem. Geol.*, 2018, **483**, 410–425.
18 M. Yang, R. L. Romer, Y. H. Yang, S. T. Wu, H. Wang, J. R. Tu, H. Y. Zhou, L. W. Xie, C. Huang, L. Xu, J. H. Yang and F. Y. Wu, *Chem. Geol.*, 2022, **593**, 120754.
19 Y. B. Cheng, C. Spandler, A. I. S. Kemp, J. W. Mao, B. Rusk, Y. Hu and K. Blake, *Am. Mineral.*, 2019, **104**, 118–129.
20 L. Gemmrich, L. Torró, J. C. Melgarejo, O. Laurent, J. Vallance and C. Chelle-Michou, *Miner. Deposita*, 2021, **56**, 1491–1520.
21 X. H. He, J. X. Zhao, R. J. Zhou, Y. X. Feng, N. Leonard, F. Li, Z. Liu, L. T. Li and S. W. Tan, *Chem. Geol.*, 2022, **609**, 121063.
22 S. T. Wu, M. Yang, Y. H. Yang, L. W. Xie, C. Huang, H. Wang and J. H. Yang, *Int. J. Mass Spectrom.*, 2020, **456**, 116394.
23 S. T. Wu, Y. H. Yang, N. M. W. Roberts, M. Yang, H. Wang, Z. W. Lan, T. Y. Li, L. Xu, C. Huang, L. W. Xie, J. H. Yang and F. Y. Wu, *Sci. China: Earth Sci.*, 2022, **65**, 1146–1160.
24 M. Yang, Y. H. Yang, S. T. Wu, R. L. Romer, X. D. Che, Z. F. Zhao, W. S. Li, J. H. Yang, F. Y. Wu, L. W. Xie, C. Huang, D. Zhang and Y. Zhang, *J. Anal. At. Spectrom.*, 2020, **35**, 2191–2203.
25 Y. H. Yang, M. Yang, H. Wang, J. H. Yang and F. Y. Wu, *Sci. China: Earth Sci.*, 2021, **64**, 187–190.
26 K. P. Jochum, U. Weis, B. Stoll, D. Kuzmin, Q. C. Yang, I. Raczek, D. E. Jacob, A. Stracke, K. Birbaum, D. A. Frick, D. Günther and J. Enzweiler, *Geostand. Geoanal. Res.*, 2011, **35**, 397–429.
27 S. T. Wu, G. Wörner, K. P. Jochum, B. Stoll, K. Simon and A. Kronz, *Geostand. Geoanal. Res.*, 2019, **43**, 567–584.
28 C. Paton, J. Hellstrom, B. Paul, J. Woodhead and J. Hergt, *J. Anal. At. Spectrom.*, 2011, **26**, 2508–2518.
29 J. D. Woodhead and J. M. Hergt, *Geostand. Geoanal. Res.*, 2005, **29**, 183–195.
30 J. D. Woodhead, J. M. Hergt, M. Shelley, S. Eggins and R. Kemp, *Chem. Geol.*, 2004, **209**, 121–135.
31 P. J. Patchett and M. Tatsumoto, *Contrib. Mineral. Petrol.*, 1981, **75**, 263–267.
32 P. A. Carr, S. Zink, V. C. Bennett, M. D. Norman and Y. Amelin, A new method for U-Pb geochronology of cassiterite by ID-TIMS applied to the Mole Granite polymetallic system, eastern Australia, *Chem. Geol.*, 2020, **539**, 119539.
33 J. N. Connelly, D. G. Ulfbeck, K. Thrane, M. Bizzarro and T. Housh, *Chem. Geol.*, 2006, **233**, 126–136.
34 M. Yang, Y. H. Yang, N. J. Evans, L. W. Xie, C. Huang, S. T. Wu, J. H. Yang and F. Y. Wu, *Geostand. Geoanal. Res.*, 2020, **44**, 543–565.
35 Y. H. Yang, H. F. Zhang, Z. Y. Chu, L. W. Xie and F. Y. Wu, *Int. J. Mass Spectrom.*, 2010, **290**, 120–126.
36 J. S. Bettencourt, R. M. Tosdal, W. B. Leite Jr and B. L. Payolla, *Precambrian Res.*, 1999, **95**, 41–67.
37 B. P. Debowski, M. I. Alves, A. C. Dos Santos, A. D. Tavares Jr and M. C. Geraldes, *Journal of the Geological Survey of Brazil*, 2019, **2**(3), 151–164.
38 S. Dewaele, Ph. Muchez, R. Bugress and A. Boyce, Geological setting and timing of the cassiterite vein type mineralization of the Kalima area (Maniema, Democratic Republic of Congo), *J. Afr. Earth Sci.*, 2015, **112**, 199–212.
39 B. Fu, J. Cliff and R. E. Zartman, *Can. J. Earth Sci.*, 2014, **51**, 485–499.
40 P. Cerny and T. S. Ercit, *Can. Mineral.*, 2005, **43**, 2005–2026.
41 D. Bradley, E. Shea, R. Buchwaldt, S. Bowring, J. Benowitz, P. O'Sullivan and A. McCauley, *Can. Mineral.*, 2016, **54**, 945–969.
42 Y. F. Bao, Y. J. Liu and X. C. Wang, *Jilin Daxue Xuebao, Xinxi Kexueban*, 2008, **27**, 56–59.
43 G. C. Li, C. Y. Feng, R. J. Wang, S. C. Ma, H. M. Li and A. S. Zhou, *Acta Geosci. Sin.*, 2012, **33**, 216–226.
44 Y. B. Gao, W. Y. Li, Z. M. Li, J. Wang, K. K. Hattori, Z. W. Zhang and J. Z. Geng, *Econ. Geol.*, 2014, **109**, 1787–1799.
45 X. H. Deng, Y. J. Chen, L. Bagas, H. Y. Zhou, Z. Zheng, S. W. Yue, H. J. Chen, H. M. Li, J. R. Tu and Y. R. Cui, *Ore Geol. Rev.*, 2017, **100**, 534–544.
46 Y. B. Gao, W. Y. Li, K. Li, B. Qian, Z. W. Zhang, A. S. Zhou, Y. S. Wu, J. W. Zhang, Z. P. Guo and Y. L. Wang, *Northwest. Geol.*, 2012, **45**(4), 229–241.
47 C. Y. Feng, Z. Zeng, D. Zhang, W. Qu, A. Du, D. Li and H. She, *Ore Geol. Rev.*, 2011, **43**, 8–25.
48 H. Q. Huang, X. H. Li, W. X. Li and Y. Liu, *Geol. J. China Univ.*, 2008, **14**, 317–333.
49 Y. Zhang, J. H. Yang, J. Y. Chen, H. Wang and Y. X. Xiang, *Lithos*, 2017, **278–281**, 166–180.
50 D. Zhang, K. D. Zhao, B. D. Wang, K. Y. Cheng, X. L. Luo, W. Zhang, Q. Li and S. Y. Jiang, *Ore Geol. Rev.*, 2020, **126**, 103758.
51 W. Zheng, J. W. Mao, C. S. Zhao, H. G. Ouyang and X. Y. Wang, *Resour. Geol.*, 2016, **66**, 63–70.
52 P. C. Hu, W. G. Zhu, H. Zhong, R. Q. Zhang, X. Y. Zhao and W. Mao, *Miner. Deposita*, 2020, **56**, 743–765.
53 W. Zheng, J. W. Mao, H. J. Zhao, H. G. Ouyang, C. S. Zhao and X. F. Yu, *Ore Geol. Rev.*, 2017, **88**, 739–752.
54 T. Iizuka and T. Hirata, *Chem. Geol.*, 2005, **220**, 121–137.
55 N. C. Chu, R. N. Taylor, V. Chavagnac, R. W. Nesbitt, M. Boella and J. A. Milton, *J. Anal. At. Spectrom.*, 2002, **17**, 1567–1574.
56 M. F. Thirlwall and R. Anczkiewicz, *Int. J. Mass Spectrom.*, 2004, **235**, 59–81.
57 H. L. Yuan, S. Gao, M. N. Dai, C. L. Zong, D. Günther, G. H. Fontaine, X. M. Liu and C. R. Diwu, *Chem. Geol.*, 2008, **247**, 100–118.
58 Z. C. Hu, Y. S. Liu, S. Gao, W. G. Liu, W. Zhang, X. R. Tong, L. Lin, K. Q. Zong, M. Li, H. H. Chen, L. Zhou and L. Yang, *J. Anal. At. Spectrom.*, 2012, **27**, 1391–1399.

